Earth and Planetary Science Letters 450 (2016) 10–19

Contents lists available at ScienceDirect

Earth and Planetary Science Letters

www.elsevier.com/locate/epsl

Signature of slab fragmentation beneath Anatolia from full-waveform tomography

Rob Govers [a,*], Andreas Fichtner [b]

[a] Department of Earth Sciences, Utrecht University, Heidelberglaan 2, Utrecht, The Netherlands
[b] Department of Earth Sciences, ETH Zurich, Sonneggstrasse 5, 8092 Zurich, Switzerland

ARTICLE INFO

Article history:
Received 1 December 2015
Received in revised form 29 April 2016
Accepted 9 June 2016
Available online xxxx
Editor: A. Yin

Keywords:
evolution of the eastern Mediterranean
seismic tomography
Aegean slab
Anatolian plateau
STEP

ABSTRACT

When oceanic basins close after a long period of convergence and subduction, continental collision and mountain building is a common consequence. Slab segmentation is expected to have been relatively common just prior to closure of other oceans in the geological past, and may explain some of the complexity that geologists have documented in the Tibetan plateau also. We focus on the eastern Mediterranean basin, which is the last remainder of a once hemispherical neo-Tethys ocean that has nearly disappeared due to convergence of the India and Africa/Arabia plates with the Eurasia plate. We present new results of full-waveform tomography that allow us to image both the crust and upper mantle in great detail. We show that a major discontinuity exists between western Anatolia lithosphere and the region to the east of it. Also, the correlation of geological features and the crustal velocities is substantially stronger in the west than in the east. We interpret these observations as the imprint in the overriding plate of fragmentation of the neo-Tethys slab below it. This north-dipping slab may have fragmented following the Eocene (about 35 million years ago) arrival of a continental promontory (Central Anatolian Core Complex) at the subduction contact. From the Eocene through the Miocene, slab roll-back ensued in the Aegean and west Anatolia, while the Cyprus–Bitlis slab subducted horizontally beneath central and east Anatolia. Following collision of Arabia (about 16 million years ago), the Cyprus–Bitlis slab steepened, exposing the crust of central and east Anatolia to high temperature, and resulting in the velocity structure that we image today. Slab fragmentation thus was a major driver of the evolution of the overriding plate as collision unfolded.

1. Introduction

The mechanical interplay between subducting and overriding lithosphere changes considerably upon entrance of continental crust into a subduction zone. Crustal fragments on the subducting plate may delaminate and be transferred to the overriding plate. Alternatively, the slab may break off altogether. As continental crust commonly arrives asynchronously at the trench in a closing oceanic basin, it is likely that a once-continuous slab becomes laterally fragmented. However, closure of the Tethyan Ocean, the largest recently disappeared basin, can be traced in tomographic images of the Earth's mantle but the evidence for lateral slab fragmentation has been limited: the Tethys slab is probably fragmented beneath the Tibetan plateau (e.g., Liang et al., 2012) and Anatolia (De Boorder et al., 1998). What remains unclear in these regions is how slab fragmentation affected the evolution of the overriding plate. We exploit new results of full-waveform tomography for the Aegean–Anatolian region to address this question (Fig. 1). A main improvement of this new technique over classical methods is that it gives an unprecedented view of both the crust and upper mantle, allowing us to make the connection between different levels. We first try to connect the imaged structures to known geological features in the uppermost crust and upper mantle. Various new features arise from this. Many of these features can be explained by a regional plate tectonic evolution involving slab fragmentation that left a footprint in the overriding plate.

2. Tomographic method

While largely inaccessible to direct observation, the Earth's interior can be probed indirectly using seismic waves excited by earthquakes. As seismic waves encounter structural heterogeneities, their propagation velocity changes, scattering and reflec-

* Corresponding author.
E-mail addresses: r.govers@uu.nl (R. Govers), andreas.fichtner@erdw.ethz.ch (A. Fichtner).

http://dx.doi.org/10.1016/j.epsl.2016.06.014
0012-821X/

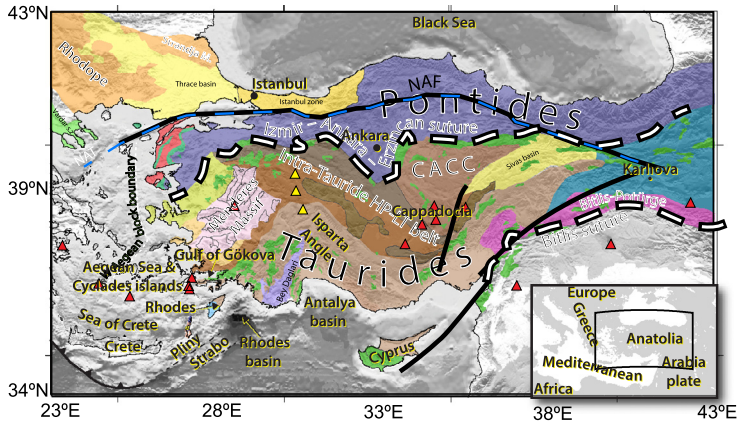

Fig. 1. Shaded relief map showing our study region, geographic names, and main tectonic units. We use "Anatolia" as a synonym for Asian Turkey. See Fig. 3 caption for details (colors in the web version of this article).

tions occur, and compressional and shear waves convert into each other. The combined effect of multiple heterogeneities produces a highly complex wave field recorded in the form of seismograms. Seismic tomography exploits the information contained in these wave field complexities to infer the structural heterogeneities from which they originated.

Advances in high-performance computing and numerical wave propagation allow us to exploit complete seismograms, including all the complexities induced by 3D-heterogeneity, using a variant of tomography often termed 'full-waveform inversion' (FWI) (e.g., Chen et al., 2007; Fichtner et al., 2009). FWI naturally combines body- and surface-wave tomography, and it accounts for the nonlinearity of the tomographic inverse problem through iterative improvements of an Earth model. New multiscale variants of FWI (Fichtner et al., 2013a) are able to jointly invert for the details of crustal and upper-mantle structure, yielding constraints in the depth interval from 10–100 km where crust–mantle interactions shape the nature of plate tectonics.

Here we offer a tectonic interpretation of a recent multi-scale FWI applied to Europe and western Asia, with a special focus on the Anatolian region where particularly dense coverage is available (Fichtner et al., 2013a). Our data set consists of 16,837 three-component seismograms, corresponding to 113 M5.0-6.8 earthquakes that occurred between 2005 and 2011 along the tectonically active margins of the Eurasian plate. Within the Anatolian region, complete seismograms are modeled and inverted in the period range from 8–200 s, ensuring that crustal and mantle structures are jointly constrained.

In the following sections, we present our tomographic model in terms of the isotropic shear velocity V_s, computed from the (Voigt) average of the elastic tensor over all angles. In terms of the SH-velocity V_{sh} and the SV-velocity V_{sv}, the isotropic velocity can be computed as $V_s^2 = 2/3V_{sh}^2 + 1/3V_{sv}^2$ (Babuska and Cara, 1991). The reference frequency in the visco-elastic model is 1 Hz. The attenuation model is QL6 (Durek and Ekström, 1996). Quantitative resolution analyses (Fichtner et al., 2013b) indicate that structures with a lateral extent of 25 km or more are resolved from the surface to around 50 km depth. Below 50 km depth, lateral resolution length increases gradually, but structures wider than 50 km are generally reliably imaged. Based on the comparison with receiver function studies, vertical resolution within the upper 50 km is estimated to be around 10 km.

To place our model into a wider context, we provide comparisons to the global lithospheric model LITHO1.0 (Pasyanos et al., 2014). We estimate that uncertainties due to anisotropy and attenuation are on the order of 0.1–0.2 km/s. These errors are, however, too small to affect our main results.

3. Results

Fig. 2 shows the tomographic result at selected depths. By using grey tone contours we attempt to maximize an objective evaluation with a level of detail that agrees with the tomographic resolution (Appendix A in Supplementary material).

3.1. Isotropic S-wave speeds in the upper mantle

We start our discussion of the results at 100 km depth because this allows us to connect our results to earlier studies. Fig. 2h displays V_s at 100 km depth. Large-scale features agree with the results from previous combined body and surface wave tomographies (e.g., Legendre et al., 2012). Much like Zhu et al. (2015), we resolve considerably more regional detail. The Aegean slab in the southwest is visible as a relatively high velocity anomaly that was identified also in previous studies (Bijwaard et al., 1998; Piromallo and Morelli, 2003) and that is coincident with the regional Wadati–Benioff zone. The sequence of horizontal slices in Movie 1 (Auxiliary Materials) demonstrates the northeastward dip of the slab in the depth range from 100 to 300 km. It also shows that the slab edge roughly aligns with the Pliny–Strabo "trenches" at the surface, supporting the interpretation of this plate boundary as a STEP fault (Govers and Wortel, 2005; Özbakır et al., 2013).

A second, separate, high velocity anomaly is visible in the depth range 25–150 km near the Turkish southwest coast. At 25 km it is located below the Gulf of Gökova, and below the Rhodes Basin in the depth range 100–150 km. The anomaly coincides with a Wadati–Benioff zone (Gessner et al., 2013). The Rhodes Basin is a very young (post-Miocene) and unusually deep basin. Özbakır et al. (2013) propose that Africa–Aegean relative motion is partly accommodated by NW directed thrusting here. This high velocity anomaly may thus correspond to a gravitational instability that developed recently along the STEP fault as was predicted by Baes et al. (2011) based on geodynamic model experiments.

In the depth range 60–160 km (Movie 1), a relatively fast anomaly is located beneath the Antalya basin and Isparta Angle. It corresponds roughly with a NE dipping Wadati–Benioff zone. Similar anomalies have been imaged in previous tomographic studies (Biryol et al., 2011). Biryol et al. (2011) interpret this anomaly as the west Cyprus slab. Their eastern segment connects all the way up to the trench to the south of Cyprus, is not expressed in the uppermost 150 km of our results. Below 270 km depth, S-wave velocities higher than 4.65 km/s are interpreted as signatures of a deeper slab that is also imaged by Biryol et al. (2011), and that they interpret as the Cyprus slab. Biryol et al. (2011) argue that the shallow Cyprus slab became fragmented recently. Relative

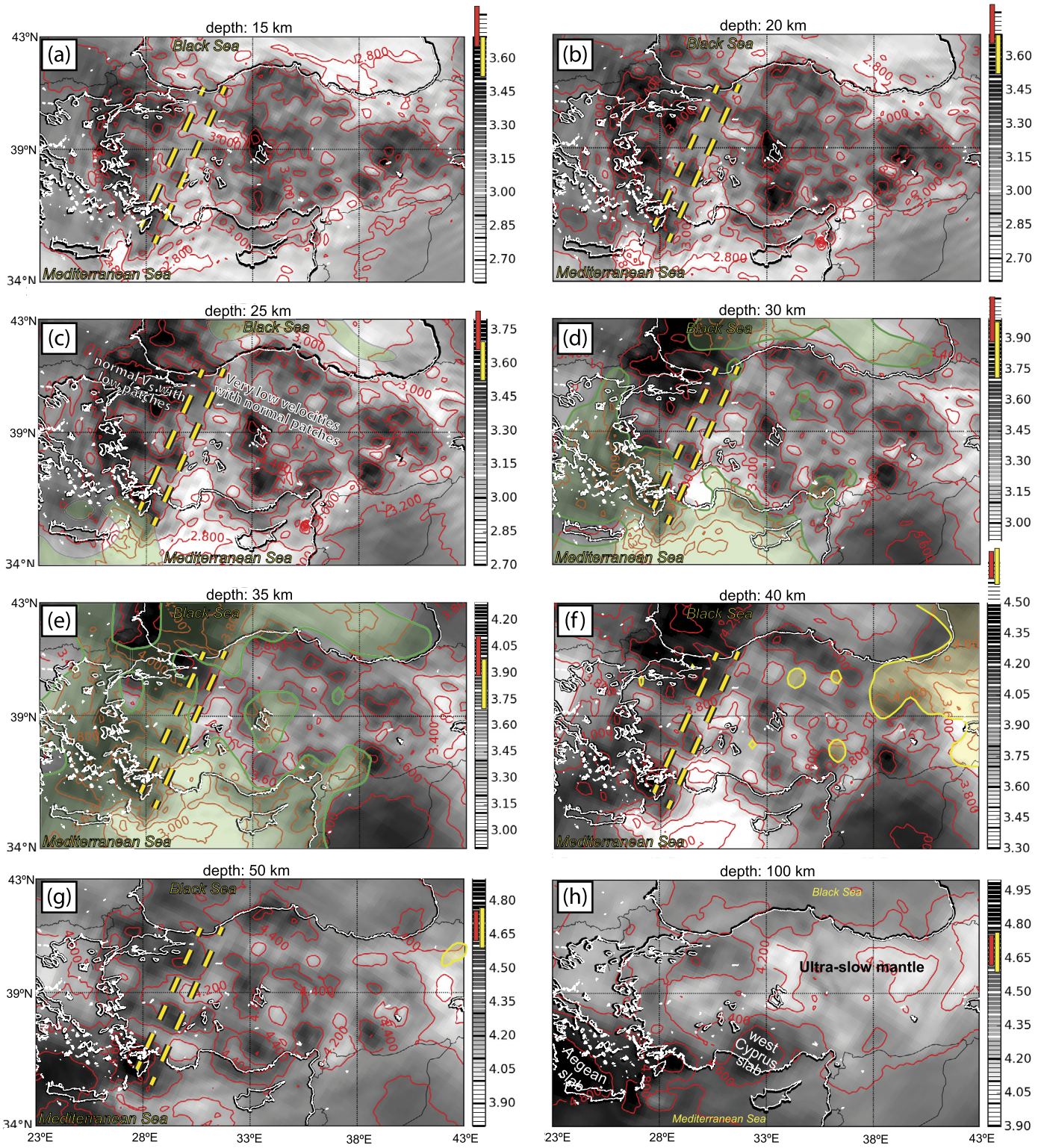

Fig. 2. Results of full-waveform inversion at different crustal and upper mantle levels in the greater Anatolia region. Grey contour colors display isotropic S-velocities; note that contour scales vary per panel. Yellow and red lines in the color scales show average S-velocities derived from LITHO1.0 (Pasyanos et al., 2014); the red line is the global continental average velocity, and the yellow line represents the continental average velocity for the Tethyan collision zone only. In panels **(a)**–**(c)** red and yellow lines represent average S-velocities for the middle crust (3751 ± 91 m/s and 3610 ± 93 m/s, respectively). In panels **(d)** and **(e)** red and yellow lines represent average S-velocities for the lower crust (4002 ± 115 m/s and 3840 ± 138 m/s, respectively). Red and yellow lines in panels **(f)**–**(h)** represent averages for the uppermost mantle (4691 ± 66 m/s and 4680 ± 89 m/s, respectively). Velocity contour lines at 200 m/s intervals are shown in red. Thick black lines with a white fill show coastlines. Thin black lines represent national boundaries. Transparent green regions in panels **(c)**–**(e)** show regions with relatively shallow Moho, i.e., here our model samples the uppermost mantle, whereas the rest of the panel displays crustal velocities. In the transparent yellow region in **(f)** the Moho is deeper than 40 km, i.e., here our model samples the lower crust, whereas the rest of the panel displays uppermost mantle velocities. Yellow dashed lines in panels **(a)**–**(g)** outline the boundary between a region of unusually low velocities with normal velocity patches in the ESE, and a region with more normal S-velocities with low-speed patches in the WNW. (For interpretation of the references to color in this figure legend, the reader is referred to the web version of this article.)

to the Aegean slab, the anomaly associated with the Cyprus slab (fragments) is weak in the uppermost 300 km (Movie 1). Previous studies demonstrated that the fast anomalies associated with the Aegean, Cyprus and Bitlis slabs merge at the bottom of the upper mantle (Bijwaard et al., 1998; Piromallo and Morelli, 2003; Biryol et al., 2011).

Away from the high-velocity anomalies, S-wave speeds are significantly slower than the global continental average in lithospheric mantle lids (thick red line in Fig. 2h). They are also much slower than the lithospheric mantle in the Cenozoic Tethyan collision zone. Ultra-slow velocities ($\leq$4.3 km/s) occur beneath part of western and central Anatolia, and below most of eastern Anatolia. Sub-crustal horizontal slices at 50–100 km give a similar, albeit more patchy impression (Movie 1). Low sub-crustal velocities were also observed in Pn-tomography studies (Al-Lazki et al., 2004; Gans et al., 2009; Mutlu and Karabulut, 2011) and in surface wave tomography studies (e.g., Salaün et al., 2012), and are commonly interpreted as thin or absent lithospheric mantle. This interpretation is corroborated by seismic attenuation studies (e.g., Al-Damegh et al., 2004).

3.2. Crust and upper mantle

Before discussing our results at more shallow levels, a few comments need to be made about the crustal thickness. As discussed in Fichtner et al. (2013a), Moho depth is well constrained in the tomographic inversion of the model. In western Turkey, the results agree with estimates of 28–40 km by Vanacore et al. (2013) and Mutlu and Karabulut (2011). In central Turkey, Moho depths of 30–40 km agree with Grad et al. (2009), Vanacore et al. (2013) and Pasyanos et al. (2014). In eastern Turkey, the Moho depth ranges between 34 and 52 km, in agreement with the findings of Vanacore et al. (2013). The Aegean Sea has a Moho depth of 32–33 km, except in the Sea of Crete where it ranges from 20 to 30 km (Endrun et al., 2008). We use the interpolated Moho depth map of Vanacore et al. (2013) (their Fig. 4) for Anatolia, in combination with the map of Grad et al. (2009) for the surrounding marine domains, to separate crustal and upper mantle domains in our horizontal cross-sections.

3.3. A large-scale velocity dichotomy

Fig. 2c shows isotropic S-velocities in the lower half of the continental crust, at 25 km. A remarkable large-scale feature is the NNE–SSW granularity. Crustal velocities are unusually low to the ESE of the yellow dashed lines, and more normal to the WNW of it. In Anatolia, smaller regions with more normal velocities float in the low-speed domain. Low-speed patches are found beneath western Turkey and the easternmost Aegean region. Our qualification of "low-speed" and "high-speed" is based here on the comparison with the average speed in the middle continental crust (Pasyanos et al., 2014; yellow or red bars in the Fig. 2c scale bar). However, in central Anatolia, to the north of Cyprus, and in western Anatolia, the crustal thickness is 35 km or less, so that it is entirely possible that we sample velocities in the lower third of the crust here, where average velocities are higher (average isotropic 4002 ± 115 m/s in continental crust, 3840 ± 138 m/s in Tethyan crust; Pasyanos et al., 2014). The consequence is that the two "normal velocity" (dark) patches along 33°E, to south of 40°N may actually be more anomalously slow than they appear to be here. Another consequence may be that velocities in particularly the Aegean region are below average. The location, shape and width ($\sim$100 km) of the boundary region between the low- and high-speed domains are somewhat dependent on the choice of velocity contours and therefore approximate. Most likely, the transition region between the low- and high-speed domains is geometrically complicated in reality, but our results allow us to only roughly constrain its location and width. We therefore represent the transition region by straight lines.

In the remainder of this section we concentrate on the vertical continuity of the velocity dichotomy between W Turkey/Aegean and central and E Anatolia. We first focus on the large-scale pattern, ignoring the patches. In the next section we turn our attention to the patches.

The horizontal cross section at 20 km depth shows a similar pattern (Fig. 2b), i.e., a normal velocity region in the WNW and a low velocity region in the ESE. Given the uncertainties in the tomography, and in the level of arbitrariness in correlating velocity contours throughout the crust, we again opt for the simplest option for the boundary, i.e., we see no clear indication for this boundary to be tilted which is why we interpret it to be approximately vertical.

At 30 km depth, the horizontal cross section through the S-velocity model samples the uppermost mantle in significant parts of Fig. 2d. Here, the color scale bar includes global and Tethyan velocity averages for the lower third of the crust. The large-scale separation of region in the WNW with more normal crustal S-velocities and a region in the ESE with low crustal velocities is still discernable, as are many of the patches in these regions.

The cross section at 35 km depth (Fig. 2e) shows that the continental Moho is shallower in the WNW than in the ESE. The boundary between these two domains coincides with the normal- to low-velocity boundary at shallower crustal levels (dashed yellow lines). In the ESE, the crustal velocities are well below the Tethyan average, and again there are patches with more normal velocities in this domain. Interestingly, isotropic S-velocities in the WNW domain are mostly significantly lower than the average value for the mantle lid (4680 ± 89 m/s).

Fig. 2f displays a horizontal cross section at 40 km depth through the velocity model. Here, we're sampling the uppermost mantle mostly, except in the east where the crust is thicker. Velocities in continental regions are below average to the WNW of the yellow dashed lines and substantially slower than the average to the ESE of them. The velocity dichotomy that we observe at 20–30 km depth thus appears to continue into the sub-crustal mantle.

The velocity contrast is only very faint at 50 km depth (Fig. 2g) and is best appreciated in the movie (Movie 1). At greater depth it is no longer visible (cf. Fig. 2h). Likewise, the velocity contrast is feebly visible at 15 km depth (Fig. 2a) and not at 10 km. We therefore conclude that a major vertical boundary beneath western Turkey is expressed in the depth range 15–50 km. The boundary is roughly 100 km wide and separates normal to low crustal and upper mantle velocities in the WNW from low to very low S-wave speeds in the ESE.

3.4. Connection to surface geological features

At shallow levels in the crust, the correlation of the tomography results to large-scale geological features along the surface is expected to increase. We therefore examine in this section whether tectonic terranes, major faults, plate boundaries and sutures, and sedimentary basins have an imprint in the tomographic results at 10 km depth. We chose 10 km because model resolution is significantly better than at 5 km depth where Rayleigh waves are relatively insensitive to variations in shear velocities.

3.4.1. Tectonic terranes

Anatolia is an amalgamation of two major tectonic terranes (Fig. 3a). The Pontides represent the southern margin of Eurasia, whereas the Central Anatolian Core Complex (CACC) and the Anatolides–Taurides derive from the southern Gondwana/Africa

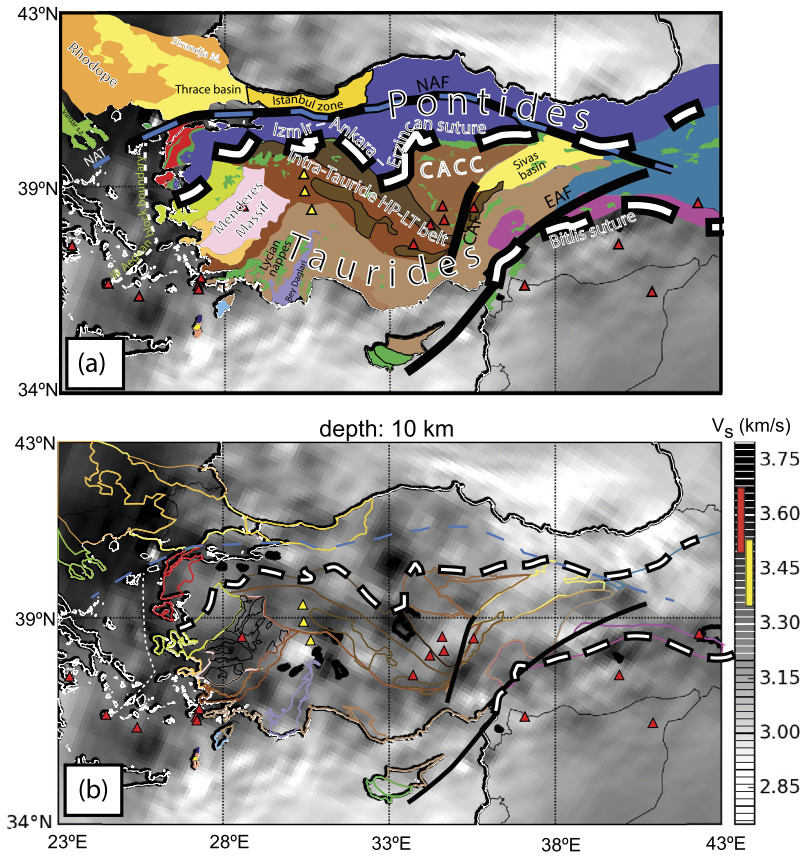

Fig. 3. (a) Tectonic map of Anatolia. Terranes to the south of the Izmir–Ankara–Erzincan (IAE) suture derive from Gondwana (Africa–Arabia) in the south. Terranes to the north of the suture derive from Laurasia in the north. The intervening ocean basin(s) closed in the early Cenozoic. Arabia collided with eastern Anatolia along the Bitlis suture in the Miocene. Since then, the North Anatolian Fault, East Anatolian Fault and Central Anatolian Fault became active. Red triangles indicate volcanoes that have been active during the Holocene, yellow triangles represent Miocene–Pliocene Kırka–Afyon–Isparta volcanics. The white dashed line in the Aegean represents the east boundary of the West Aegean block. The Intra-Tauride HP-LT belt consists of the Tavsanli zone (dark brown) in the north and the (slightly lower grade) Afyon zone (brown). Abbreviations: CACC = Central Anatolian Core Complex, CAF = Central Anatolian Fault, EAF = East Anatolian Fault, NAF = North Anatolian Fault, NAT = North Aegean Trough. **(b)** Outline of tectonic units and their correlation with isotropic S-velocities at 10 km depth (grey scale contours). Thick lines in the scale bar show average S-velocities of the upper crust; the red line is the global continental average velocity (3584 ± 89 m/s), the yellow line represents the average velocity for the continental Tethyan collision zone only (3443 ± 92 m/s). (For interpretation of the references to color in this figure legend, the reader is referred to the web version of this article.)

continent. During the Mesozoic, Gondwana–Eurasia convergence was accommodated by (mostly) northward subduction of the intervening Neo-Tethys ocean and regional back-arc basins (e.g., Schmid et al., 2008). Diachronous closure ensued in phases from the Late Cretaceous in the Dinarides until Miocene in eastern Anatolia. Juxtaposed terranes are separated by major crustal sutures in the present-day geological record; 1) the Vardar-Intra Pontides suture between the Istanbul–Rhodope–Strandja terrane in the north and the Pelagonian-Pontides/Sakarya terranes in the south; 2) the Izmir–Ankara–Erzincan suture between the Pontides terrane in the north and the Taurides/CACC in the south; 3) The Bitlis suture between the Taurides in the north and Arabia in the south. The Inner Taurides suture between the CACC in the NE and the Taurides to the SW is relevant in the context of central Anatolia.

Fig. 3b shows the tomographic model at 10 km depth. The result displays slower-than-average velocities with patches of more normal S-wave velocities in most of Anatolia and surrounding regions (Fig. 3).

We investigate the correlation with regional tectonic terranes from west to east. Such correlation is inherently restricted by the fact that (relatively thin) nappes are significant elements in the surface geology, and that the vertical extent of the underlying elements is poorly constrained by direct observation. In the Cyclades and further north, the boundary between low velocities in the west and normal velocities in the east roughly follows the east boundary of the West Aegean block of Walcott and White (1998). This boundary includes the Mid-Cycladic Lineament, but its tomographic expression does not agree with a strike-slip offset (e.g., Philippon et al., 2014). Inspection of the results at 15–55 km depth (Fig. 2, Figs. B2 and B3) shows that the northern part of the boundary persists throughout the crust, but not into the upper mantle. S-wave velocities are nearly uniformly lower than average in the Aegean domain and Greece to the west of this line.

The SW–NE oriented normal-velocity band in the eastern Aegean (centered beneath the Cycladic island of Amorgos) correlates with high-temperature metamorphic core complexes (MCCs) (including Dilek Peninsula) in the SW of it (Jolivet and Brun, 2010, and references therein). Surprisingly, the surface exposures of these MCCs continue further to the WNW (Cycladic islands Tinos, Andros, Syros, Almyropotamos), but here we find no expression in the tomographic results. The SW–NE normal-velocity band is semi-continuous with the core of the Menderes Massif (Fig. 3a; Bozkurt and Oberhänsli, 2001). The expression of the east Cycladic MCCs is absent deeper than 10 km (Fig. 2, Movie 1). The vertical cross section in Appendix B (Supplementary material) is complementary to cross-section A–A′ in Fichtner et al. (2013a). It illustrates that the normal velocities that, at the surface, correspond to lower crustal rocks, appear unconnected to the lower crust. The eastern Sea of Crete hosts a normal velocity patch (restricted to the 10 km level) that does not correlate with known geological features.

In the north part of the Aegean region, the boundary between low (south) and normal (north) velocities coincides with the North

Aegean Trough at 10 km depth, i.e., the WSW extension of the North Anatolian Fault (NAF) into the Aegean region. As the total offset on the NAF is less than 100 km, it is unlikely that this contrast results from Miocene–Recent strike slip. Normal velocities to the north of this boundary continue beneath the Rhodope Massif and the Vardar suture zone. In the east, this normal velocity region ends beneath the Thrace basin. The lower velocity domain extends further to the north of the Aegean and into the Rhodope at deeper crustal levels, where the correlation with the North Aegean Trough is absent.

A string of more normal velocity patches appear to follow the Taurides limestone belt along the southern boundary of the Intra-Tauride belt (Afyon–Bolkardağ) at 10 km depth. If existent, the correlation is weak and it does not extend to deeper levels (Figs. B2–B3).

In the rest of central Anatolia and in eastern Anatolia, the correlation between the tomographic results and the main tectonic terranes is weak or absent.

3.4.2. Sutures, major faults and volcanoes

We next examine the correlation with sutures and faults in order of geological importance. Mesozoic–Early Cenozoic subduction at the Izmir–Ankara–Erzincan crustal suture (Fig. 3a) eventually resulted in closure of the main Neo-Tethyan ocean basin between the Pontides (Eurasia) and Anatolides–Taurides (Gondwana) (e.g., Robertson et al., 2012). The geological suture aligns with a velocity contrast that persists throughout the crust into the uppermost mantle (10–50 km) between 37°E and 40°E: it separates very low velocities to the north of it from low velocity to the south. Further to the west, the correlation is insignificant.

The active major plate boundary between Eurasia and Turkey is the North Anatolian Fault (NAF). It traces the Izmir–Ankara–Erzincan crustal suture between 37°E and 40°E, i.e., at 10 km depth the NAF correlates with a velocity contrast here and further to the east near Karliova (Fichtner et al., 2013b). Delph et al. (2015a) find a similar pattern. Geological observations are very clear in that the right-lateral offset on the NAF is on the order of 85 km (Hubert-Ferrari et al., 2002). Such offset is not recognizable in the tomographic result and it is therefore more likely that observable velocity contrasts result from Mesozoic–Oligocene juxtaposition of different tectonic terranes, i.e., our findings support the notion that the NAF is a relatively recent (∼11–13 Ma) feature that developed largely along pre-existing terrane boundaries (Şengör et al., 2005). At deeper crustal levels (15–40 km), we observe velocity contrasts across the NAF between 33°E and 40°E (Fig. 2, Figs. B2 and B3, Movie 1; Delph et al., 2015b). A velocity contrast is not discernible below the crust; in the depth range 50–70 km, a low velocity anomaly roughly straddles the eastern part of the NAF (36–40°E). Low Pn velocities are imaged in roughly the same location by Al-Lazki et al. (2004), Gans et al. (2009) and Mutlu and Karabulut (2011), although details differ. In our velocity model, the NAF does not correlate with significant velocity contrasts to the west of 33°E where, interestingly, the NAF bifurcates.

HP-LT terranes to the SW of the Inner-Tauride suture are located structurally below unmetamorphosed units to the NE; this attests to Late Cretaceous convergence here. The Inner-Tauride suture does however not correlate with a significant velocity contrast at 10 km depth (Fig. 3). The surface correlation of the Afyon Zone to the Bolkardağ unit in the east (Okay, 1984) is not expressed in the deeper structure. Similarly, the surface correlation of the Afyon Zone to the Lycian Nappes and the Menderes Massif in the west does not have a deep expression either. This may be unsurprising given that these units are relatively thin. Much-lower-than-average velocities in the SW and lower-than-average velocities in the NE signify a velocity contrast across the NW of the Inner-Tauride suture at 15 and 20 km depth (Figs. B2 and B3).

The Neo-Tethys ocean between Arabia and Anatolia closed during the Miocene along the Bitlis, or Assyrian, suture (Yılmaz, 1993). The surface Bitlis suture separates a series of north–south velocity contrasts at 10 km depth, and deeper in the crust (Figs. B2 and B3). Sub-crustal low velocities cross the surface exposure of the Assyrian Suture. This result differs from the contrast across the suture that Gans et al. (2009) image using Pn. Mutlu and Karabulut (2011) also do not image a contrast in their Pn results. Given that our FWI includes a wide range of seismic phases including Pn, and that we are not restricted by the assumption of mild Moho topology gradients, we have more confidence in our result.

Active volcanoes (last 10,000 yrs) correlate with low to very low velocities throughout the crust. The Miocene–Pliocene Kırka–Afyon–Isparta volcanic centers (Savaşçin and Oyman, 1998) also overlie low crustal velocity zones. The sub-crustal low-velocity anomaly beneath the south Kirşehir block coincides with the middle Miocene–Quaternary Cappadocia volcanic province (visible in Pn anomaly in Gans et al., 2009 and Mutlu and Karabulut, 2011).

3.4.3. Basins

In Fig. B4, we explore the possibility that low velocities, potentially smeared downwards in the tomography, are associated with regional continental basins. The basin depth and fill, and therefore its expression in the seismic velocities, will vary laterally within a basin so we do not necessarily expect a single (slow) velocity per basin. Even with this consideration in mind, the correlation between the location of basins and slow velocities is poor: very slow velocities occur where there are no basins, and more normal velocities below basins. We therefore conclude that basins are not the cause for the low to very low regional velocities. A likely cause for the lack of correlation is that the basins are relatively shallow: e.g., the basement of the western Sivas basin is located at about 2500 m below the topography (Yılmaz and Yılmaz, 2006), which is too shallow to significantly affect the average velocity.

Within the low-velocity domain in the ESE, the ultra-low velocity anomaly below the Isparta Angle is an outstanding vertical feature that exists in the crust from 15–30 km and uppermost mantle from 35–50 km (Delph et al., 2015a). At crustal levels, this Isparta anomaly continues horizontally into the East Mediterranean basin to the south in a region that is bounded by the Pliny–Strabo trenches and southern Cyprus. As we will elaborate further below, this likely represents the recent accretionary plate contact.

3.4.4. Other notable features

In a context of low velocities at the hundreds of km's horizontal scale, the normal-velocity-patch around 33°E, 39°N stands out throughout the crust (10–30 km) and uppermost mantle (35–50 km) as a continuous and near-vertical feature. Given its location below the lake, we refer to it as the Tuz Gölü patch. It is collocated with part of (the Afyon terrane of) the Intra-Tauride HP/LT belt, immediately south of the IAE suture (Fig. 3). Another, less pronounced normal-velocity-patch in the depth range 15–55 km is situated around 33.5°E, 37°N, nearly above the Cyprus slab (Fig. 2, Movie 1). It sits at the southern end of the Intra-Taurides HP/LT belt. For both patches, the correlation with neither the basins nor the tectonic map is significant.

In a context of normal velocities at the large scale, a WNW striking low-velocity zone is present in the crust and uppermost mantle (15–55 km) along a line (26°E, 40.2°N) to (29°E, 39°N). This corresponds roughly to the northern boundary of the Bornova Flysch and the Menderes Massif with the Intra-Taurides belt (Fig. 3), and is oriented perpendicular to the dichotomy boundary (dashed lines in Fig. 3).

Beneath Crete, sub-crustal velocities at 35 km depth show a gradual decrease from west to east from ∼3.6 km/s to 3.4 km/s, and a sharper decrease offshore to the east. Our model thus does

not capture an increase in velocities over Crete as found by Endrun et al. (2008).

3.4.5. Summary

Velocity contrasts in the upper crust correlate with tectonic terrane boundaries in the Aegean region. The Izmir–Ankara–Erzincan suture aligns with S-velocity contrasts in the east, and not in the west. The Bitlis suture in east Anatolia is expressed as a velocity contrast throughout the crust. The weak correlation in particularly central Anatolia, but also east Anatolia, is remarkable and is an important ingredient for the slab fragmentation scenario that we present below.

4. From structure to process

Any scenario that explains the velocity dichotomy and the weak correlation of shallow geological features and tomography should agree with the overall constraints on the regional tectonic evolution. We therefore review this first.

4.1. Regional tectonic evolution

Africa/Arabia and Eurasia converged since before the Eocene. In this large-scale context, the geology of the Aegean region and west Anatolia clearly documents major extension of the overriding plate since then (e.g., Jolivet and Brun, 2010; van Hinsbergen et al., 2010), i.e., mainly horizontal tectonics. The extension varies from up to ∼350 km in the Aegean region (Gautier et al., 1999), to ∼150 km (in the Menderes Massif in) in western Turkey. This extension is, and probably was, primarily driven by southwestward rollback of the Aegean slab (McClusky et al., 2000).

Contrastingly, central Anatolia shows relatively little horizontal deformation since the Eocene, and has a footprint of mostly vertical tectonics due to mantle delamination in the Late Miocene (Bartol and Govers, 2014). The post-Eocene evolution of eastern Anatolia documents continued convergence and accretion, delamination and slab break-off (Keskin, 2003), i.e., both horizontal and vertical deformation.

4.2. Aegean extensional domain

The region to the west of the velocity dichotomy is bounded by another boundary further to the west, at least in the crust. The boundary partially follows the east boundary of the West Aegean block of Walcott and White (1998). Normal crustal velocities (with low-velocity patches) in west Turkey transition into lower-than-average velocities in the Aegean region and eastern Greece. At shallow levels, the transition correlates roughly with Cenozoic amounts of extension; highly extended regions and core complexes (Jolivet and Brun, 2010) in the west, and less extended regions in the east, in western Turkey. Deeper in the crust (15–25 km) however, the lower velocity domain extends further to the north of the Aegean, and the correlation with crustal extension is less apparent. The uniformity of the isotropic S-wave velocities is remarkable here, and suggestive of a cause that is independent of the well-established geological complexity of the region.

Crustal or lithospheric extension brings rocks closer to the surface. Since seismic velocities normally increase with depth, this results in higher velocities in extended crust than in normal crust, contrary to what we observe in the Aegean region. Then there is the temperature effect: deeper rocks are hotter. If the extension is fast enough, the rocks will hardly cool in the process and result in an increased temperature gradient and surface heat flow. This we see in the Aegean region. Thermal models demonstrate that the heat flow decays on time scales of millions of years. This is an expression of cooling of the crust or lithosphere. The point here is that crustal or lithospheric extension results in cooling of rocks, and not in heating. Another consequence of extension is that it puts higher-grade rocks (with higher seismic velocities) closer to the surface. Low velocities in our westernmost region are thus not a direct consequence of crustal or lithospheric extension.

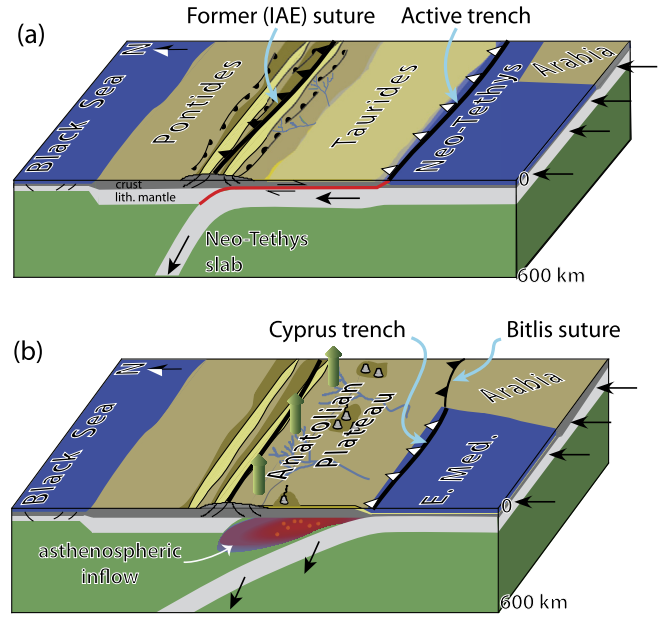

Fig. 4. Schematic overview of the lithospheric evolution of central and eastern Anatolia (modified after Bartol and Govers, 2014). **(a)** In the period (Eocene–Miocene) after closure of the Izmir–Ankara–Erzincan (IAE) suture, convergence of Africa/Anatolia w.r.t. Eurasia was accommodated by flat subduction from the trench to the south of the Taurides. Minor shortening occurred within the Taurides. **(b)** Steepening of the Cyprus–Bitlis slab followed after closure at the Bitlis suture around ∼16 Ma. This resulted in the exposure of the central and east Anatolian crust to hot asthenospheric material, providing buoyancy and heat. Consequence was uplift and volcanism, and lowering of crustal and upper mantle velocities (colors in the web version of the article).

Mantle convection above a (retreating) slab may increase the heat flow into the overriding plate (Currie and Hyndman, 2006). Within a couple of million years, such a perturbation would evoke higher rock temperatures in most of the crust. This is thus a viable explanation for slower velocities, but it does not explain the (partial) coincidence of low velocities and more highly extended regions. One possibility is that if the convective heat input from the mantle is laterally variable (as it would be for narrow slabs like the Aegean slab), overriding plate extension would concentrate in the warmer regions.

Water lowers the S-wave speed and reduces rock viscosity. A similar argumentation can therefore be used to explain the observations: (laterally variable) water input from dehydrating slab into the crust. The imprint of water on seismic velocities would be particularly significant at high (homologous) temperatures because water lowers the melting temperature, so that the fraction of partial melt would increase.

4.3. Central and East Anatolian delamination domain

Bartol and Govers (2014) integrate surface geological data and the observation of a single slab in the deeper mantle (Hafkenscheid et al., 2006) into a scenario for the combined evolution of eastern and central Anatolia. Key to this scenario is the notion that roughly 400 km of Eocene–Miocene convergence between Africa and the Pontides was accommodated by the Cyprus–Bitlis trench to the south of central and east Anatolia (Fig. 4a). The ultra-slow velocity anomaly beneath the Isparta Angle that continues to the

ESE is a likely consequence of accretion along this plate boundary (Delph et al., 2015a). Bartol and Govers (2014) propose that horizontal/flat subduction occurred beneath the Anatolides–Taurides during this period, and that the slab sank deeper into the mantle below the Izmir–Ankara–Erzincan suture zone.

In the next phase between 20 and 15 Ma, slab steepening and delamination exposed the Anatolide–Taurides crust and upper mantle to asthenospheric temperatures, resulting in uplift of the (central and east) Anatolian plateau and in volcanic activity (Fig. 4b). Bartol and Govers (2014) test this scenario using a thermal/flexural model to come to the conclusion that the model predictions agree quantitatively with present-day observations.

We interpret the low-velocity domain to the east of the dichotomy boundary to result from this Miocene delamination. The replacement of the sub-crustal lid by hot asthenosphere would have rapidly heated the crust, added volatiles including water, and would have resulted in the observed low-velocity pattern that crosses most terrane boundaries. Eclogitization of at least the lower crust is unlikely given the limited depth/pressure 40 km/1 GPa max. The region that was exposed to high temperatures crosses most geological boundaries, which explains why velocities correlate poorly to shallow geological features.

4.4. Evolution of the slab tear: a scenario

The dichotomy boundary that we identify here represents the transition between the extensional domain in the west and the delamination domain in the east. Given the critical role played by the Aegean and Cyprus–Bitlis slabs in the development of the crust we present a scenario for the evolution of the involved crusts and lithospheres.

Fig. 5a schematically shows the large-scale tectonic setting since Eocene collision of the Anatolide–Taurides (including the CACC) with the Sakarya terrane. In the west, the Aegean slab rolled back resulting in (variable) extension in the Aegean and west Turkey back-arc. In keeping with the scenario of Bartol and Govers (2014; Fig. 4), subduction beneath central Anatolia occurred at the trench to the south of central Anatolia, where the slab subducted horizontally. The slab sank deeper into the mantle beneath the former suture in the north. This eastern slab remained stationary until the Miocene, whereas the western slab migrated to the south, i.e., continual tearing of the slab was required to accommodate this. This was similar to a STEP (Govers and Wortel, 2005), yet quite different because the tearing processes occurred well below the Anatolian crust, i.e., the STEP was not active along the surface. In the cartoon picture in Fig. 5a we assumed the tear to be narrow, which is not necessarily correct. The brown zone represents a wide shear zone in the crust that spawned from this narrow tear. Here, anti-clockwise vertical axis rotations of crustal blocks originated along the transition between the two regions.

When did the slab fragment? Present-day slabs are commonly not segmented despite the fact that they contain major lateral discontinuities (fracture zones, continental ridges). To fragment a slab is thus not mechanically easy and requires a substantial trigger. One potential trigger may have been the Cretaceous–late Eocene collision of the CACC with the IASZ. One observation in support of such interpretation is that the western boundary of the CACC corresponds roughly with the NNE end of our dichotomy boundary. Collision of the CACC lead to a jump of the trench to the south of Central Anatolia around the Eocene–Oligocene, and to the onset of flat-slab subduction beneath Central Anatolia (Bartol and Govers, 2014). The offset between the Aegean trench in the west, and the new Cyprus trench in the east would have been approximately 400 km in a (roughly) north–south direction. The transition would have occurred in or near western Anatolia, i.e., within an east–west distance of roughly 400 km. If the Neo-Tethys slab had remained continuous it would thus have been strongly flexed/curved, which in our opinion is possible but unlikely given its old (Triassic) age. Also, a continuous slab would kinematically require eastward thrusting here, and there is little evidence for this. We consider slab fragmentation in the Eocene–Oligocene more likely therefore. This timing agrees with contrasting deformation regimes in Aegean and Central Anatolian parts of the overriding plate from (at least) 35 to 16 Ma; structural evidence in the Çankırı basin (north of the CACC) indicates compression continuing into the Early Miocene (Kaymakci, 2000). The onset of back-arc extension in the Aegean and western Turkey is uncertain. The oldest, Eocene, estimate results from attributing extension in the Rhodope massif to slab rollback. A younger, Oligocene, age corresponds with the onset of extension in the Cyclades. We thus suspect that the configuration of Fig. 5a existed from at least 35 Ma to 16 Ma.

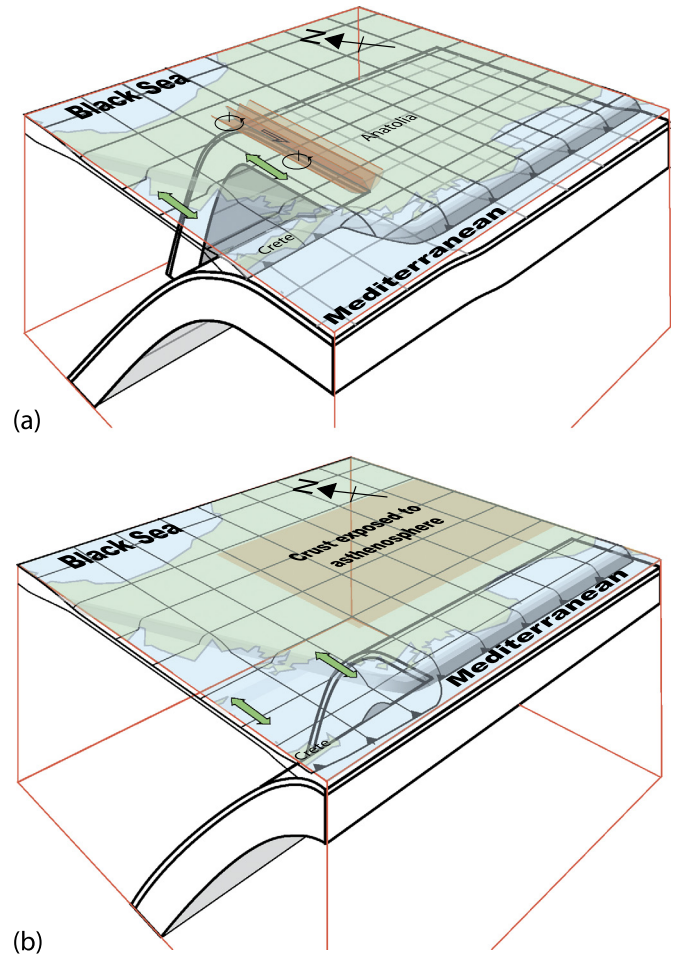

Fig. 5. Two-stage lithospheric evolution of central Anatolia and the Aegean region. The scenario depicted here combines the evolution for central and east Anatolia (Fig. 4) with the Aegean evolution. **(a)** Eocene–Miocene: fragmentation of the neo-Tethys slab made it possible for the Aegean slab to start rolling back while horizontal subduction of the Cyprus–Bitlis slab continued beneath east and central Anatolia – this required continual slab tearing below the Anatolian crust. Differential motion required by Aegean back-arc extension (green arrows) resulted in a wide shear zone (brown) in the Anatolia crust. **(b)** Post 16 Ma steepening of the Cyprus–Bitlis slab resulted in detachment beneath the Anatolia plateau (Fig. 4), eventually leading to STEP tectonics after 5 Ma. (For interpretation of the references to color in this figure legend, the reader is referred to the web version of this article.)

Fig. 5b schematically shows the Miocene–Pliocene tectonic setting. Collision of Arabia at the Bitlis suture resulted in steepening of the Bitlis–Cyprus slab (Bartol and Govers, 2014). Following breakoff of the Bitlis slab fragment, this eastern slab developed into the Cyprus slab. Steepening exposed the central and eastern Anatolian crust to asthenospheric temperatures and, in our inter-

pretation, lead to the low velocity crustal footprint there. Bartol and Govers (2014) show that asthenospheric buoyancy suffices to drive Miocene uplift of the Anatolian plateau. The boundary between our two domains coincides with the NNE-ward extension of the Pliny–Strabo STEP fault, the boundary of the Menderes and Lycian Nappes, and passes beneath the Kirka–Afyon–Isparta Volcanic Field. This suggests that the Aegean slab (segment) showed roll-back whereas the slab further east did not. The imaged dichotomy boundary does not represent the tear in the subducting lithosphere. Rather, it represents the footprint in the Anatolian lithosphere of the fragmented Tethyan slab beneath it. The western and central Anatolian lithosphere probably had a limited size lithospheric mantle, which is why the dichotomy boundary does not extend very deep (15–50 km). Seismic velocities are slowest immediately to the east of the dichotomy boundary, which we attribute to enhanced vertical upwelling and heat flow into the Anatolian crust along the western edge of the Bitlis–Cyprus slab during steepening.

Bartol and Govers (2014) estimate that detachment beneath central Anatolia started in the early Miocene between 15 and 20 Ma. Jolivet et al. (2013) surmise that vertical tearing of a once-intact slab would have facilitated accelerated SW-ward retreat of the Hellenic slab during the Miocene. This may have accelerated tectonic processes in the Aegean and western Turkey; e.g., clockwise rotation of the external Hellenides started around 15 Ma (Kissel and Laj, 1988), rotation of the Menderes Massif started ∼16 Ma (van Hinsbergen et al., 2010), and rollback velocity of the Aegean slab may have increased from slow (<1 cm/yr) to faster (3 cm/yr) around 13 Ma (Philippon et al., 2014).

Savaşçin and Oyman (1998) interpreted southward younging of Kırka (21–17 Ma), Afyon (14–8 Ma) and Isparta (4.7–4 Ma) volcanic centers in terms of segmentation of the Aegean and Cyprus arcs. Dilek and Altunkaynak (2009) propose that this volcanic sequence represents the volcanic trace of a STEP beneath western Turkey. Karaoğlu and Helvacı (2014) conclude that the isotopic composition agrees with a transition from subduction to slab-tear related volcanism. De Boorder et al. (1998) speculated that a lateral edge of the Aegean slab below W Turkey might have caused mineralization in and around the Menderes Massif. Based on the counterclockwise rotation of the southern Menderes–Bey Daglari, van Hinsbergen et al. (2010) suggest that this STEP may have existed since the late Oligocene. As explained before, we think that the STEP was not active in the Anatolian crust (so that consequently no STEP fault developed) but we concur with the interpretation that the segmentation of the slab may have caused the inception and migration of these volcanic centers.

How did the tear evolve after the Miocene? We surmise that the sub-crustal tear migrated from beneath the Anatolian crust into the east Mediterranean basin around the Pliocene where it became a proper STEP. In this interpretation, the Pliny–Strabo STEP fault (Özbakır et al., 2013) is the prolongation of the sub-crustal tear. The oldest segment of the Pliny–Strabo STEP fault occurs in the NE in the Rhodes Basin (a transtensional basin without Messinian evaporates). Locally, the age of the STEP fault is thus younger than 5.3 Myr. This would thus be roughly the time when the eastern edge of the Aegean slab emerged from beneath the crust of western Turkey.

5. Conclusions

A major vertical boundary beneath western Turkey is expressed in the tomographic results between 15–50 km depth. This dichotomy boundary is roughly 100 km wide and separates normal to low crustal and upper mantle velocities in the WNW from low to very low S-wave speeds in the ESE. The accretion boundary from Isparta angle to Cyprus is imaged as ultra-slow velocities. Our observations, when interpreted in the context of the regional tectonic evolution, are consistent with Eocene fragmentation of the Aegean–Cyprus–Bitlis slab followed by slab roll-back in the west and horizontal subduction in the east. After collision in east Anatolia around 16 Ma, steepening of the Cyprus–Bitlis slab resulted in uplift and heating of the central and east Anatolia crust. In this scenario, the dichotomy boundary is understood to be the result of major heating of the central and east Anatolia crust, in contrast with extension of the west Anatolia and Aegean crust. Eocene slab fragmentation thus was a major driver of the regional evolution as collision developed.

Supplementary material

Supplementary material including Appendix A and B, and Movie 1 can be found online at http://dx.doi.org/10.1016/j.epsl.2016.06.014.

Acknowledgements

We thank Rinus Wortel for comments on an earlier version of the manuscript and Douwe van Hinsbergen for his help with the tectonic map. We are grateful to Laurent Jolivet and an anonymous reviewer for their constructive comments.

References

Al-Damegh, K., Sandvol, E., Al-Lazki, A., Barazangi, M., 2004. Regional seismic wave propagation (Lg and Sn) and Pn attenuation in the Arabian Plate and surrounding regions. Geophys. J. Int. 157, 775–795. http://dx.doi.org/10.1111/j.1365-246X.2004.02246.x.

Al-Lazki, A.I., Sandvol, E., Seber, D., Barazangi, M., Turkelli, N., Mohamad, R., 2004. Pn tomographic imaging of mantle lid velocity and anisotropy at the junction of the Arabian, Eurasian and African plates. Geophys. J. Int. 158, 1024–1040. http://dx.doi.org/10.1111/j.1365-246X.2004.02355.x.

Babuska, V., Cara, M., 1991. Seismic Anisotropy in the Earth. Springer Netherlands, Dordrecht.

Baes, M., Govers, R., Wortel, R., 2011. Subduction initiation along the inherited weakness zone at the edge of a slab: insights from numerical models. Geophys. J. Int. 184, 991–1008. http://dx.doi.org/10.1111/j.1365-246X.2010.04896.x.

Bartol, J., Govers, R., 2014. A single cause for uplift of the Central and Eastern Anatolian plateau? Tectonophysics 637, 116–136. http://dx.doi.org/10.1016/j.tecto.2014.10.002.

Bijwaard, H., Spakman, W., Engdahl, E., 1998. Closing the gap between regional and global travel time tomography. J. Geophys. Res. 103, 30055–30078.

Biryol, C., Beck, S.L., Zandt, G., Özacar, A.A., 2011. Segmented African lithosphere beneath the Anatolian region inferred from teleseismic P-wave tomography. Geophys. J. Int. 184, 1037–1057. http://dx.doi.org/10.1111/j.1365-246X.2010.04910.x.

Bozkurt, E., Oberhänsli, R., 2001. Menderes Massif (Western Turkey): structural, metamorphic and magmatic evolution – a synthesis. Int. J. Earth Sci. 89, 679–708.

Chen, P., Zhao, L., Jordan, T.H., 2007. Full 3D tomography for the crustal structure of the Los Angeles region. Bull. Seismol. Soc. Am. 97, 1094–1120.

Currie, C., Hyndman, R., 2006. The thermal structure of subduction zone back arcs. J. Geophys. Res. 111, B08404.

De Boorder, H., Spakman, W., White, S., Wortel, M., 1998. Late Cenozoic mineralization, orogenic collapse and slab detachment in the European Alpine Belt. Earth Planet. Sci. Lett. 164, 569–575.

Delph, J.R., Biryol, C.B., Beck, S.L., Zandt, G., Ward, K.M., 2015a. Shear wave velocity structure of the Anatolian Plate: anomalously slow crust in southwestern Turkey. Geophys. J. Int. 202 (1), 261–276.

Delph, J.R., Zandt, G., Beck, S.L., 2015b. A new approach to obtaining a 3D shear wave velocity model of the crust and upper mantle: an application to eastern Turkey. Tectonophysics 665, 92–100.

Dilek, Y., Altunkaynak, S., 2009. Geochemical and temporal evolution of Cenozoic magmatism in western Turkey: mantle response to collision, slab break-off, and lithospheric tearing in an orogenic belt. In: Hinsbergen, D., Edwards, M.A., Govers, R. (Eds.), Collision and Collapse at the Africa–Arabia–Eurasia Subduction Zone. Geological Society of London, pp. 213–233.

Durek, J.J., Ekström, G., 1996. A radial model of anelasticity consistent with long-period surface wave attenuation. Bull. Seismol. Soc. Am. 86, 144–158.

Endrun, B., Meier, T., Lebedev, S., Bohnhoff, M., Stavrakakis, G., Harjes, H.-P., 2008. S-velocity structure and radial anisotropy in the Aegean region from surface wave dispersion. Geophys. J. Int. 174, 593–616. http://dx.doi.org/10.1111/j.1365-246X.2008.03802.x.

Fichtner, A., Kennett, B.L.N., Igel, H., Bunge, H.-P., 2009. Full seismic waveform tomography for upper-mantle structure in the Australasian region using adjoint methods. Geophys. J. Int. 179, 1703–1725.

Fichtner, A., Trampert, J., Cupillard, P., Saygin, E., Taymaz, T., Capdeville, Y., Villaseñor, A., 2013a. Multiscale full waveform inversion. Geophys. J. Int. 194, 534–556. http://dx.doi.org/10.1093/gji/ggt118.

Fichtner, A., Saygin, E., Taymaz, T., Cupillard, P., Capdeville, Y., Trampert, J., 2013b. The deep structure of the North Anatolian Fault Zone. Earth Planet. Sci. Lett. 373, 109–117. http://dx.doi.org/10.1016/j.epsl.2013.04.027.

Gans, C.R., Beck, S.L., Zandt, G., Biryol, C.B., Ozacar, A.A., 2009. Detecting the limit of slab break-off in central Turkey: new high-resolution Pn tomography results. Geophys. J. Int. 179, 1566–1572. http://dx.doi.org/10.1111/j.1365-246X.2009.04389.x.

Gautier, P., Brun, J.-P., Moriceau, R., Sokoutis, J., Martinod, J., Jolivet, L., 1999. Timing, kinematics and cause of Aegean extension: a scenario based on a comparison with simple analogue experiments. Tectonophysics 315, 31–72.

Gessner, K., Gallardo, L.A., Markwitz, V., Ring, U., Thomson, S.N., 2013. What caused the denudation of the Menderes Massif: review of crustal evolution, lithosphere structure, and dynamic topography in southwest Turkey. Gondwana Res. 24, 243–274. http://dx.doi.org/10.1016/j.gr.2013.01.005.

Govers, R., Wortel, M., 2005. Lithosphere tearing at STEP faults: response to edges of subduction zones. Earth Planet. Sci. Lett. 236, 505–523.

Grad, M., Tiira, T., ESC Working Group, 2009. The Moho depth map of the European Plate. Geophys. J. Int. 176, 279–292.

Hafkenscheid, E., Wortel, M., Spakman, W., 2006. Subduction history of the Tethyan region derived from seismic tomography and tectonic reconstructions. J. Geophys. Res. 111 (B8). http://dx.doi.org/10.1029/2005JB003791.

Hubert-Ferrari, A., Armijo, R., King, G., Meyer, B., Barka, A., 2002. Morphology, displacement, and slip rates along the North Anatolian Fault, Turkey. J. Geophys. Res. 107, 2235. http://dx.doi.org/10.1029/2001JB000393.

Jolivet, L., Brun, J.-P., 2010. Cenozoic geodynamic evolution of the Aegean. Int. J. Earth Sci. 99, 109–138.

Jolivet, L., Faccenna, C., Huet, B., Labrousse, L., Le Pourhiet, L., Lacombe, O., Lecomte, E., Burov, E., Denèle, Y., Brun, J.-P., Philippon, M., Paul, A., Salaün, G., Karabulut, H., Piromallo, C., Monié, P., Gueydan, F., Okay, A.I., Oberhänsli, R., Pourteau, A., Augier, R., Gadenne, L., Driussi, O., 2013. Aegean tectonics: strain localisation, slab tearing and trench retreat. Tectonophysics 597–598, 1–33. http://dx.doi.org/10.1016/j.tecto.2012.06.011.

Karaoğlu, Ö., Helvacı, C., 2014. Isotopic evidence for a transition from subduction to slab-tear related volcanism in western Anatolia, Turkey. Lithos 192–195, 226–239. http://dx.doi.org/10.1016/j.lithos.2014.02.006.

Kaymakci, N., 2000. Tectono-stratigraphical evolution of the Çankırı Basin (Central Anatolia, Turkey). Geologica Ultraiectina. Ph.D. thesis. Utrecht University.

Keskin, M., 2003. Magma generation by slab steepening and breakoff beneath a subduction-accretion complex: an alternative model for collision-related volcanism in Eastern Anatolia, Turkey. Geophys. Res. Lett. 30, 8046. http://dx.doi.org/10.1029/2003GL018019.

Kissel, C., Laj, C., 1988. The Tertiary geodynamic evolution of the Aegean arc: a paleomagnetic reconstruction. Tectonophysics 146, 183–201.

Legendre, C.P., Meier, T., Lebedev, S., Friederich, W., Viereck-Götte, L., 2012. A shear wave velocity model of the European upper mantle from automated inversion of seismic shear and surface waveforms. Geophys. J. Int. 191, 282–304.

Liang, X., Sandvol, E., Chen, Y.J., Hearn, T., Ni, J., Klemperer, S., Shen, Y., Tilmann, F., 2012. A complex Tibetan upper mantle: a fragmented Indian slab and no southverging subduction of Eurasian lithosphere. Earth Planet. Sci. Lett. 333–334, 101–111. http://dx.doi.org/10.1016/j.epsl.2012.03.036.

McClusky, S., Balassanian, S., Barka, A., Demir, C., Ergintav, S., Georgiev, I., Gurkan, O., Hamburger, M., Hurst, K., Kahle, H., 2000. Global Positioning System constraints on plate kinematics and dynamics in the eastern Mediterranean and Caucasus. J. Geophys. Res. 105, 5695–5719.

Mutlu, A.K., Karabulut, H., 2011. Anisotropic Pn tomography of Turkey and adjacent regions. Geophys. J. Int. 187, 1743–1758.

Okay, A.I., 1984. Distribution and characteristics of the north–west Turkish blueschists. Geol. Soc. (Lond.) Spec. Publ. 17, 455–466. http://dx.doi.org/10.1144/GSL.SP.1984.017.01.33.

Özbakır, A.D., Şengör, A.M.C., Wortel, M.J.R., Govers, R., 2013. The Pliny–Strabo trench region: a large shear zone resulting from slab tearing. Earth Planet. Sci. Lett. 375, 188–195. http://dx.doi.org/10.1016/j.epsl.2013.05.025.

Pasyanos, M.E., Masters, T.G., Laske, G., Ma, Z., 2014. LITHO1.0: an updated crust and lithospheric model of the Earth. J. Geophys. Res. 119, 2153–2173. http://dx.doi.org/10.1002/2013JB010626.

Philippon, M., Brun, J.-P., Gueydan, F., Sokoutis, D., 2014. The interaction between Aegean back-arc extension and Anatolia escape since Middle Miocene. Tectonophysics 631, 176–188. http://dx.doi.org/10.1016/j.tecto.2014.04.039.

Piromallo, C., Morelli, A., 2003. P wave tomography of the mantle under the Alpine–Mediterranean area. J. Geophys. Res. 108, 2065. http://dx.doi.org/10.1029/2002JB001757.

Robertson, A.H.F., Parlak, O., Ustaömer, T., 2012. Overview of the Palaeozoic–Neogene evolution of Neotethys in the Eastern Mediterranean region (southern Turkey, Cyprus, Syria). Pet. Geosci. 18, 381–404. http://dx.doi.org/10.1144/petgeo2011-091.

Salaün, G., Pedersen, H.A., Paul, A., Farra, V., Karabulut, H., Hatzfeld, D., Papazachos, C., Childs, D.M., Pequegnat, C., SIMBAAD Team, 2012. High-resolution surface wave tomography beneath the Aegean–Anatolia region: constraints on upper-mantle structure. Geophys. J. Int. 190, 406–420. http://dx.doi.org/10.1111/j.1365-246X.2012.05483.x.

Savaşçin, M.Y., Oyman, T., 1998. Tectono-magmatic evolution of alkaline volcanics at the Kırka–Afyon–Isparta Structural Trend, Sw Turkey. Turk. J. Earth Sci. 7, 201–214.

Schmid, S., Bernoulli, D., Fügenschuh, B., Matenco, L., Schefer, S., Schuster, R., Tischler, M., Ustaszewski, K., 2008. The Alpine–Carpathian–Dinaridic orogenic system: correlation and evolution of tectonic units. Swiss J. Geosci. 101, 139–183.

Şengör, A., Tüysüz, O., Imren, C., Sakinç, M., Eyidogan, H., Görür, N., Le Pichon, X., Rangin, C., 2005. The North Anatolian fault: a new look. Annu. Rev. Earth Planet. Sci. 33, 37–112.

van Hinsbergen, D.J.J., Dekkers, M.J., Bozkurt, E., Koopman, M., 2010. Exhumation with a twist: paleomagnetic constraints on the evolution of the Menderes metamorphic core complex, western Turkey. Tectonics 29, TC3009. http://dx.doi.org/10.1029/2009TC002596.

Vanacore, E.A., Taymaz, T., Saygin, E., 2013. Moho structure of the Anatolian Plate from receiver function analysis. Geophys. J. Int. 193, 329–337. http://dx.doi.org/10.1093/gji/ggs107.

Walcott, C.R., White, S.H., 1998. Constraints on the kinematics of post-orogenic extension imposed by stretching lineations in the Aegean region. Tectonophysics 298, 155–175. http://dx.doi.org/10.1016/S0040-1951(98)00182-6.

Yılmaz, Y., 1993. New evidence and model on the evolution of the southeast Anatolian orogen. Geol. Soc. Am. Bull. 105, 251–271.

Yılmaz, A., Yılmaz, H., 2006. Characteristic features and structural evolution of a post collisional basin: The Sivas Basin, Central Anatolia, Turkey. J. Asian Earth Sci. 27, 164–176.

Zhu, H., Bozdag, E., Tromp, J., 2015. Seismic structure of the European upper mantle based on adjoint tomography. Geophys. J. Int. 201, 18–52. http://dx.doi.org/10.1093/gji/ggu492.